

Following Ion Diffusion in Solution

S. Rondot, J. Cazaux, O. Aaboubi, J. P. Chopart, A. Olivier

An x-ray projection microscope equipped with a charge-coupled device camera allows direct observation of zinc (Zn^{2+}) ions diffusing in aqueous hydrochloric acid solution during the corrosion of zinc foil and pellets. Time series of microradiographic images with a lateral resolution on the order of 10 micrometers allow observation of the time and spatial evolution of the colorless Zn^{2+} ions in solution without any previous treatment. The concentration distribution of the ions can be quantified from these images. This technique should find applications in the biology, chemistry, and electrochemistry of aqueous solutions, allowing direct observation of the behavior and concentration fluctuations of medium or heavy ions moving in a weakly absorbing medium.

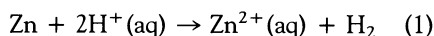
The main advantage of x-ray microscopy (XRM) is the ability to see inside thick, optically opaque specimens, even those in a liquid or gaseous environment. Another advantage, related to x-ray matter interaction, is the sensitivity in the detection of medium or heavy elements immersed in a light elemental matrix.

The use of shadow XRM to observe time-dependent phenomena is associated with the development of modern signal-detection and signal-processing devices such as the computer-controlled charge-coupled device (CCD) camera, which produces digital images within a few seconds, compared to the few minutes required by conventional photographic plates. This technique, developed without the need of focusing elements, is also characterized by a large field depth.

Fick's equations are invariably used in theoretical studies of atomic diffusion in solids (1) and liquids (2); however, they can be analytically solved for only simple geometries and boundary conditions. Conventional methods of experimental study—for example, the use of an electron microprobe in studies of heterogeneous solid-solid diffusion—require the diffusion process to be stopped for analysis (3). Consequently, such measurements strongly perturb the experiment. Two methods are commonly used to study particle diffusion in a liquid during corrosion: In the first technique, the diffusing particle must be labeled, and in the other, one has to evaluate the concentration of solution samples taken periodically with a chemical or electrochemical measurement method (4).

In this report, we present a technique for the direct observation of a corrosion process by visualization of the diffusion of ions coming from the oxidation of a metal. This type of process has a time evolution long enough to be observed by absorption XRM. The approach is similar to that followed by Rothman *et al.* (5), who used high-resolu-

tion XRM to investigate cell biology, and by Anderson *et al.* (6), whose results from x-ray scanning microradiography led to a local diffusion coefficient for ions in aqueous solution within a glassfrit (porous glass). We directly observed Zn^{2+} ion diffusion during the corrosion process of zinc (in the metallic form) by a hydrochloric acid solution, following the well-known reaction



From a series of microradiographs taken periodically, one can follow the diffusion process during its development.

We used an x-ray projection microscope derived from a conventional scanning electron microscope equipped with a cooled CCD camera (7, 8). The advantages of this detector are its speed, its good linearity, and its wide dynamic range (ratio of saturation signal to readout noise; up to 3×10^4). The x-ray beam is generated by the bombardment of a metallic target with a primary electron beam whose energy can be varied from 1 to 30 keV. Different targets, placed side by side on a movable target holder, permit variation of the energy of the incoming photons without any intervention in the vacuum chamber, and a movable specimen holder permits observation of different parts of the sample by translation in the xyz directions.

The lateral resolution depends on the position of the specimen, the dimension of the x-ray source S (about $1 \mu m$), and the size D (about $25 \mu m$) of each detecting element of the x-ray detector (phosphor, fiber optic bundle, and CCD camera) (9). We achieved a lateral resolution on the order of $10 \mu m$. The detection limit for heavy atoms embedded in a weakly absorbing medium may reach 1 in 10^4 and even 1 in 10^5 in some cases (10).

Because microradiographs are acquired and stored in digital form, they lend themselves naturally to direct measurement and quantitative analysis of the specimen absorptivity at each pixel (11). Maps of μt for

the specimen can be derived with the Beer law [$I = I_0 \exp(-\mu t)$, where I is intensity, μ is the linear absorption coefficient, and t the thickness of the specimen] from three successive images: the first, B, with neither the specimen nor the illumination (to obtain the dark current of the camera), the second, E, with the x-ray beam but not the specimen (to obtain the incident photon intensity), and the third, I, with the incident beam and the specimen. The logarithm of the intensity ratio $(E - B)/(I - B)$ permits the derived values of μt to be related to each pixel of the camera (12).

Because of the nature of our x-ray microscope, the specimen is placed in the vacuum chamber. Study of a time-dependent chemical reaction in a liquid required the design of an environmental chamber (hermetic solution cell), which holds a specimen in solution at atmospheric pressure (Fig. 1). To build this cell, we followed Anderson *et al.* (6), Watanabe *et al.* (13) (who observed human blood cells with a soft x-ray microscope), and Pine and Gilbert (14) (who observed dendrites and axons in a neuron with a scanning transmission x-ray microscope). Our cell, made of polytetrafluoroethylene (PTFE), has two parts, which facilitates the introduction of the metallic sample. Two PTFE pipes connect the inside of the cell with the outside of the microscope by means of a feed-through between the vacuum chamber and the outside. This permits one to control the onset of the reaction by injecting the reactive solution after having found the zone of the cell to be observed and allowing the gases contained in the cell to be evacuated.

In our first experiment, we used a pure zinc metal disk 3 mm in diameter and 1 mm thick to approximate one-dimensional diffusion (15). The hydrochloric acid solution (36% by weight) contained glycerol, which increased the viscosity of the solution and, therefore, slowed the diffusion, avoiding

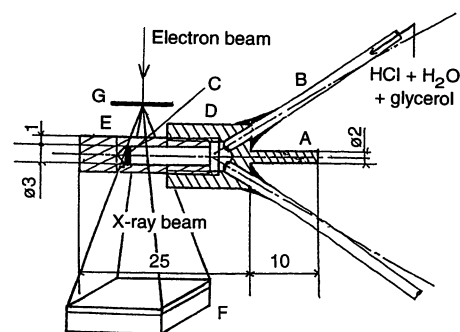


Fig. 1. Schematic diagram of the solution cell. (A) Support allowing the fixing of the cell in the moving specimen holder, (B) PTFE pipe; (C) Zn foil, and (D and E) PTFE walls. Experimental arrangement: (F) detector and (G) target holder. The indicated dimensions (ϕ indicates diameter) are in millimeters.

LASSI-LECS, Groupe de Recherche Surfaces et Matériaux, Université de Reims, UFR Sciences, BP347, 51062 Reims Cedex, France.

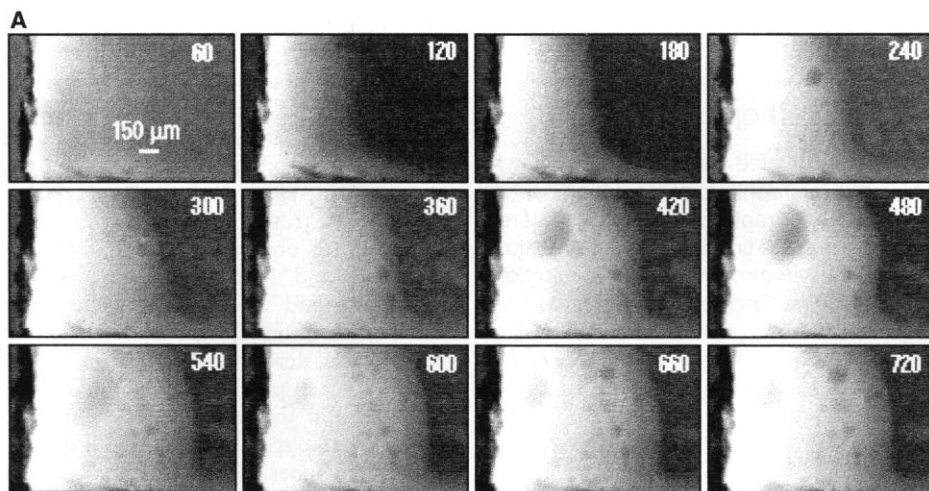


Fig. 2. (A) Corrosion of a zinc plane electrode (in black on the left of each image) set in contact with a hydrochloric acid and glycerol solution. Microradiographs were obtained by subtracting pixel by pixel the initial μt image (acquired at $t = 0$ before any chemical reaction) from the successive μt images (acquired at the indicated times in seconds during the chemical reaction). Light areas correspond to the strong x-ray absorption of the Zn^{2+} ions relative to that of the PTFE and dilute acid; dark regions characterize weaker absorption. **(B)** Diagrammatic representation. Experimental conditions: target, Mo; $E_0 = 29$ keV; $I_0 = 0.48 \mu A$.

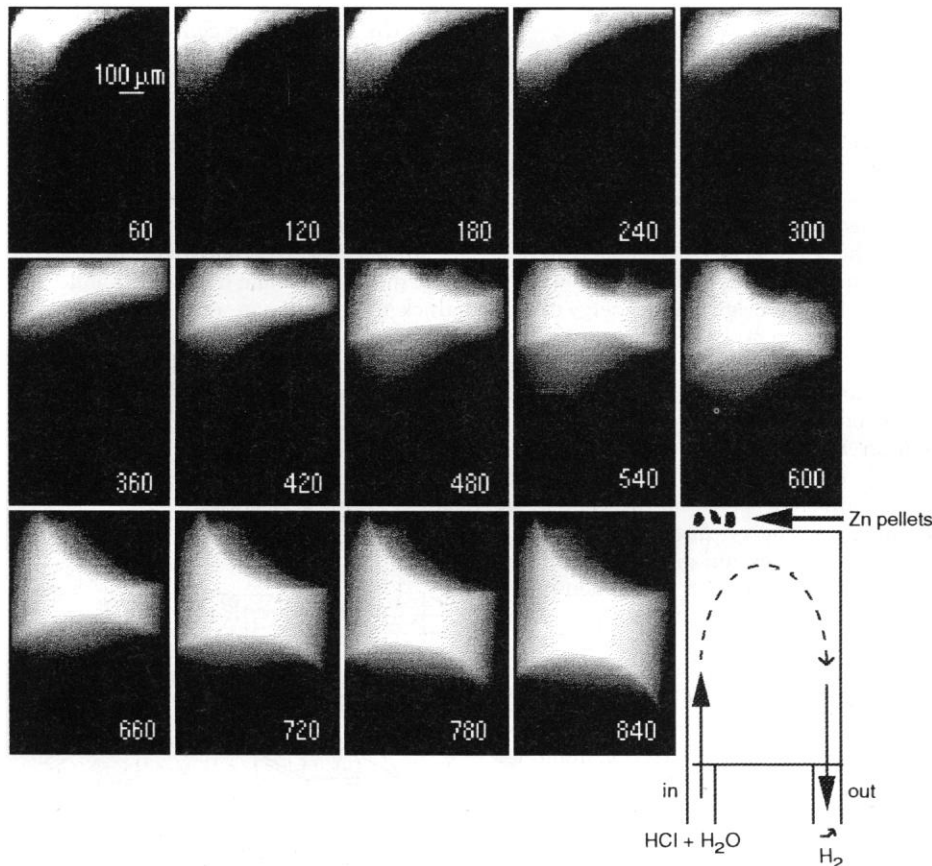
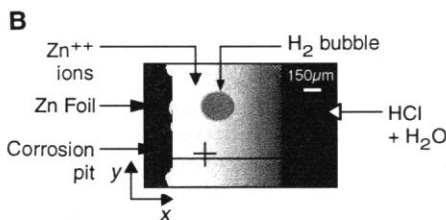


Fig. 3. General case showing diffusion of Zn^{2+} ions in a turbulent medium, limited by the walls of the cell (on left and right) and by H_2 bubbles (on top and bottom). The drawing at bottom right represents the configuration used. These images are obtained with the same mathematical process described in Fig. 2A. Experimental conditions: target, Mo; $E_0 = 29$ keV; $I_0 = 0.65 \mu A$.

convection effects near the cell walls. For the second experiment, we used pure zinc pellets and the same hydrochloric acid solution but without glycerol, to show what happens in a general case. Inside the cell, the experimental conditions (pressure, 1 atm; temperature, 293 K; $pH_{acid} < 2$; redox potential of Zn^{2+} compared with Zn, $-0.76V$ versus a normal hydrogen electrode) are those indicated by the potential/pH diagram of pure zinc, given by Pourbaix (16) for the corrosion of zinc.

We acquired 12 microradiographs of the flat disk geometry (Fig. 2) and 14 of the pellet geometry (Fig. 3). A period of 1 min separates the beginning of each image with an acquisition time of 30 s per image. We subtracted, pixel by pixel, the initial μt image (taken before any chemical reaction) from each μt image taken during the chemical reaction to eliminate the contribution of the absorption of the cell walls and of the

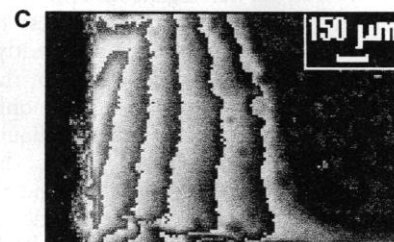
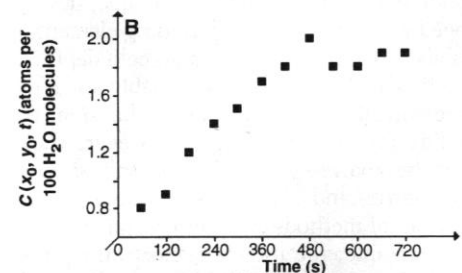
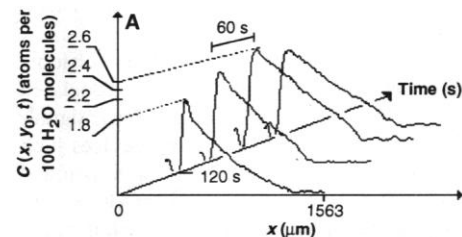


Fig. 4. (A) Evolution of a given concentration profile ($y_0 = 300 \mu m$, black line in Fig. 2B) as a function of time for four successive images taken before $t = 300$ s. **(B)** Variation of the local concentration of Zn^{2+} ions for a given pixel ($x_0 = 545 \mu m$ and $y_0 = 313 \mu m$, black cross in Fig. 2B). The change of slope at $t = 480$ s suggests the influence of other additional phenomena (such as convection) on the diffusion process, but the uncertainty of the measurements ($\pm 5\%$) does not permit claims about oscillation effects. **(C)** Isoconcentration lines of the Zn^{2+} ions in solution, deduced from the image in Fig. 2A taken at $t = 300$ s.

dilute acid solution. The microradiographs show the evolution of the ions diffusing from the metal to the solution.

The small black zones on the left of each image in Fig. 2A, caused by corrosion pits on the metallic sheet, show the progressive erosion of the metal (negative absorption because of the subtraction). Light regions in the center of the images show the diffusion process, and dark zones correspond to hydrogen (H_2) bubbles, which reduce the layer thickness of the Zn^{2+} ions and locally decrease the x-ray absorption. We do not see, as was naively expected, a front of Zn^{2+} ions moving perpendicular to the zinc electrode because, in fact, this chemical reaction is associated with complicated microscopic phenomena, such as the creation of a turbulent medium caused by the gas release. Therefore, this experiment demonstrates that this phenomenon is a complex process that cannot be studied with a one-dimensional Fick's law.

In the reaction with the zinc pellets (Fig. 3), we see the evolution of a front of Zn^{2+} ions, limited by the walls of the cell, complicated by the production and movement of H_2 bubbles and by the concentration gradient [decreases from the top left of each image (where the zinc pellets were situated) to the bottom right]. These images show what happens in a general case, without any particular geometry for the metallic specimen. The spherical edges of the front give rise to two menisci (observed from $t = 360$ s). These menisci result from the formation of H_2 bubbles. All of these images show the influence of the gas release in the creation of a turbulent medium that leads to heterogeneous diffusion.

To quantify the distribution of the Zn^{2+} ions moving into the liquid, we obtain μ t maps for each stage of the diffusion and convert them into concentration maps. It is possible to see how a given concentration profile $C(x, y_0, t)$ (Fig. 4A) or a local concentration $C(x_0, y_0, t)$ at a given point (x_0, y_0) (Fig. 4B), expressed in zinc atoms per H_2O molecule, changes with time. We can also delimit isoconcentration lines on each initial microradiograph (Fig. 4C).

Our technique, characterized by its ease of operation (a modified scanning electron microscope), good sensitivity, and sufficient spatial resolution for this type of study, offers the possibility of evaluating the local concentration of the solvated species, even in a colorless solution, such as zinc in hydrochloric acid. We believe that this technique can be adapted to a wide field of applications, including the visualization of ionic species migration during electrochemical processes, the diffusion of ionic particles in a porous medium, or the diffusion of K^+ , Na^+ , and Ca^{2+} ions in biological materials with a lateral resolution of a few micrometers.

REFERENCES

1. J. Philibert, *Atom Movement: Diffusion and Mass Transport in Solids* (Les Editions de Physique, Les Ulis, France, 1991).
2. A. Moelwyn Hughes, *The Chemical Statics and Kinetics of Solutions* (Academic Press, London, 1971), chap. 5.
3. S. Rondot, J. Cazaux, D. Erre, D. Mouze, P. Trebbia, paper presented at the Fourth International Conference on X-ray Microscopy, Chernogolovka, Russia, 20 to 24 September 1993.
4. J. Benard, A. Michel, J. Philibert, J. Talbot, *Métallurgie Générale* (Masson, Paris, ed. 2, 1991), pp. 416–417.
5. S. Rothman, K. K. Gonez, B. W. Loo Jr, in *X-ray Microscopy III*, A. G. Michette, G. R. Morrison, C. J. Buckley, Eds. (Springer-Verlag, Berlin, 1992), pp. 373–383.
6. P. Anderson, S. E. P. Dowker, J. C. Elliott, G. H. Dibdin, *ibid.*, pp. 435–437.
7. X. Thomas, J. Cazaux, D. Erre, D. Mouze, P. Collard, *ibid.*, pp. 190–194.
8. J. Cazaux *et al.*, paper presented at Euromat '93, 3rd European Conference on Advanced Materials and Processes, Paris, June 1993.
9. D. Erre, thesis, University of Reims (1993).
10. J. Cazaux, *Microsc. Microanal. Microstruct.* **4**, 513 (1993).
11. H. Ade *et al.*, *Science* **258**, 972 (1992).
12. D. Erre, D. Mouze, X. Thomas, J. Cazaux, in *Progress in Digital X-ray Projection Microscopy*, P. B. Kenway *et al.*, Eds. (Institute of Physics Conference Ser. 130, IOP Publ., London, 1993), p. 567.
13. N. Watanabe *et al.*, *Jpn. J. Appl. Phys.* **31**, L1571 (1992).
14. J. Pine and J. R. Gilbert, in (5), pp. 384–387.
15. J. O'M. Bockris and A. K. N. Reddy, *Modern Electrochemistry* (Plenum, New York, 1970), vol. 1.
16. M. Pourbaix, *Atlas d'Equilibres Electrochimiques à 25°C* (Gauthier-Villars, Paris, 1963).

4 November 1993; accepted 7 February 1994

From Static to Kinetic Friction in Confined Liquid Films

Günter Reiter, A. Levent Demirel, Steve Granick*

The transition from rest to sliding contact of atomically smooth solids separated by molecularly thin liquid films was studied. The films could be deformed nearly reversibly to a large fraction of the film thickness. The modulus of elasticity and yield stress were low, considerably less than for a molecular crystal or glass in the bulk. The transition to dissipative sliding was typically (but not always) discontinuous. The dissipative stress was then nearly velocity-independent. The similar response of monolayers strongly attached to the solid surfaces, presenting a well-defined interface for sliding, suggests that the physical mechanism of sliding may involve wall slip.

Not enough is understood about friction (1–5). This impedes progress not only on workaday problems of tribology but also on other complex dynamical problems such as earthquakes. An essential fact to appreciate is that solid bodies in contact are nearly always lubricated, either by liquids or additives that are intentionally added or by condensed vapors. However, confined liquids were recently found to exhibit patterns of friction normally associated with the deformation of solids. This result, first proposed in the engineering literature (6–8), has now also emerged for films that are molecularly thin (9, 10). However, in all of these experiments the displacements were large, too large to investigate decisively the transition from static to kinetic friction.

A surface forces apparatus with oscillatory shear attachment was used (10, 11). In previous work we investigated the perturbed liquid-like response of thicker confined liquid films (5, 10); here we investigate the solidity (4, 5, 9, 10) of thinner

films. The liquid of interest was confined between two circular parallel sheets of atomically smooth mica whose diameter was vast ($\approx 10 \mu\text{m}$) compared to the molecularly thin distance between them. The film thickness and area of flattened contact were measured by multiple-beam interferometry. Sinusoidal shear forces were applied by a piezoelectric element. A second sensor piezoelectric element was used to detect the resulting response, which was compared with the force required to deform this element when no liquid was present (12). The temperature was 27°C.

The contributions of the mechanical response of the apparatus, especially of the glue that attached the mica to the rest of the device (11), were calibrated with the mica surfaces in dry adhesive contact. Measurements with confined liquids were then analyzed with the use of a model in which the calibrated apparatus response coupled mechanically with the thin-film sample (12). With regard to the uncertainties of calibration, a conservatively low bound of glue stiffness was assumed. Consequently, deformations of the thin-film samples might be larger (perhaps by up to 50%) than those we describe below, but not smaller.

Materials Research Laboratory and Department of Materials Science and Engineering, University of Illinois, Urbana, IL 61801, USA.

*To whom correspondence should be addressed.